

## Supporting Information

### **Room-temperature sensing performance of binary Co-Zn doped MoS<sub>2</sub>/graphite composite toward ppb-level NO<sub>2</sub>**

Jin-Le Fan<sup>a,b</sup>, Xue-Feng Hu<sup>a,b,\*</sup>, Wei-Wei Qin<sup>a,b</sup>, Ming-Zhou<sup>a,b</sup>, Yan-Song Liu<sup>a,b</sup>,  
Sheng Cheng<sup>c</sup>, Shou-Jing Gao<sup>a,b</sup>, Li-Ping Tan<sup>a,b</sup>, Gui-Qiang Wang<sup>a</sup>, and Wei  
Zhang<sup>a,b,\*</sup>

<sup>a</sup> Anhui Province Key Laboratory of Measuring Theory and Precision Instrument, School of Instrument Science and Optoelectronics Engineering, Hefei University of Technology, Hefei 230009, Anhui, P. R. China

<sup>b</sup> Academy of Optoelectronic Technology, Special Display and Imaging Technology Innovation Center of Anhui Province, Hefei University of Technology, Hefei, Anhui Province, 230009, P. R. China

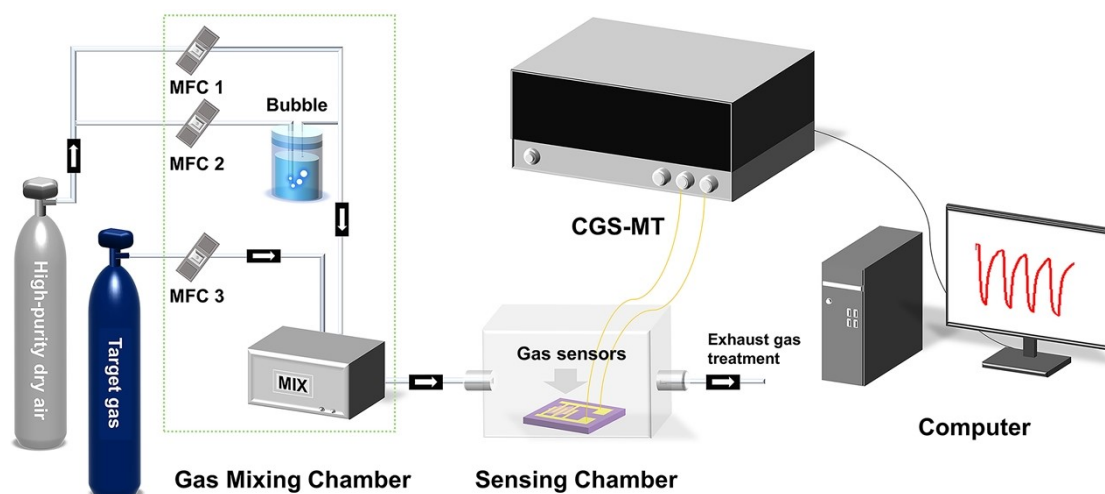
<sup>c</sup> Instrumental Analysis Center, Hefei University of Technology, Hefei, Anhui, 230009, P. R. China

\*Corresponding authors: [xuefeng.hu@hfut.edu.cn](mailto:xuefeng.hu@hfut.edu.cn) (X. Hu) and [zhangw@hfut.edu.cn](mailto:zhangw@hfut.edu.cn) (W. Zhang)

The room-temperature sensing performance of the sensors was measured by an intelligent gas-sensing platform (Elite Tech Co. Ltd, China) with High-purity dry air (HPDA) as background gas. Note that all initial gases are in the standard 4 L cylinders with a purity larger than 99.9% before they are adjusted to a determined concentration. Then, the target gases were achieved by adjusting the ratio of target gases to the carrier gas (High-purity dry air (HPDA)) via the computer-controlled mass flow controllers (MFC), and the total flow rate of the gas mixture was  $300 \text{ mL}\cdot\text{min}^{-1}$ . According to the

equation: 
$$C_1 = \frac{F_0}{F_0 + F_1} \cdot C_0$$
 (where  $C_1$  is the mixed target gas concentration,  $C_0$  is the standard gas concentration in the cylinder, and  $F_0$  and  $F_1$  are the flow rates of target gas and HPDA, respectively. The sum of  $F_0$  and  $F_1$  is  $300 \text{ mL}\cdot\text{min}^{-1}$ .), when  $C_0$  is 300 ppm  $\text{NO}_2$ , and  $F_0$  and  $F_1$  are controlled to be 5 and  $295 \text{ mL}\cdot\text{min}^{-1}$ , respectively,  $C_1$  is expected to be 5 ppm. The other  $\text{NO}_2$  gases with concentrations of 0.05 ppm, 0.1 ppm, 0.3 ppm, 0.5 ppm, 1 ppm, and 3 ppm and the other gases of 5 ppm NO, 50 ppm  $\text{NH}_3$ , 100 ppm  $\text{H}_2$ , 50 ppm CO, and 50 ppm ethanol were obtained in the same way.

Note that in the study of the effect of humidity toward  $\text{NO}_2$ , the dry air was divided into two ways, and one way was fed into the bubble to get humidity gas. Then, the stable relative humidity (RH) values were obtained by adjusting the mass flow ratios of dry and humidity gases.



**Scheme S1.** Schematic diagram of the intelligent gas sensing platform.

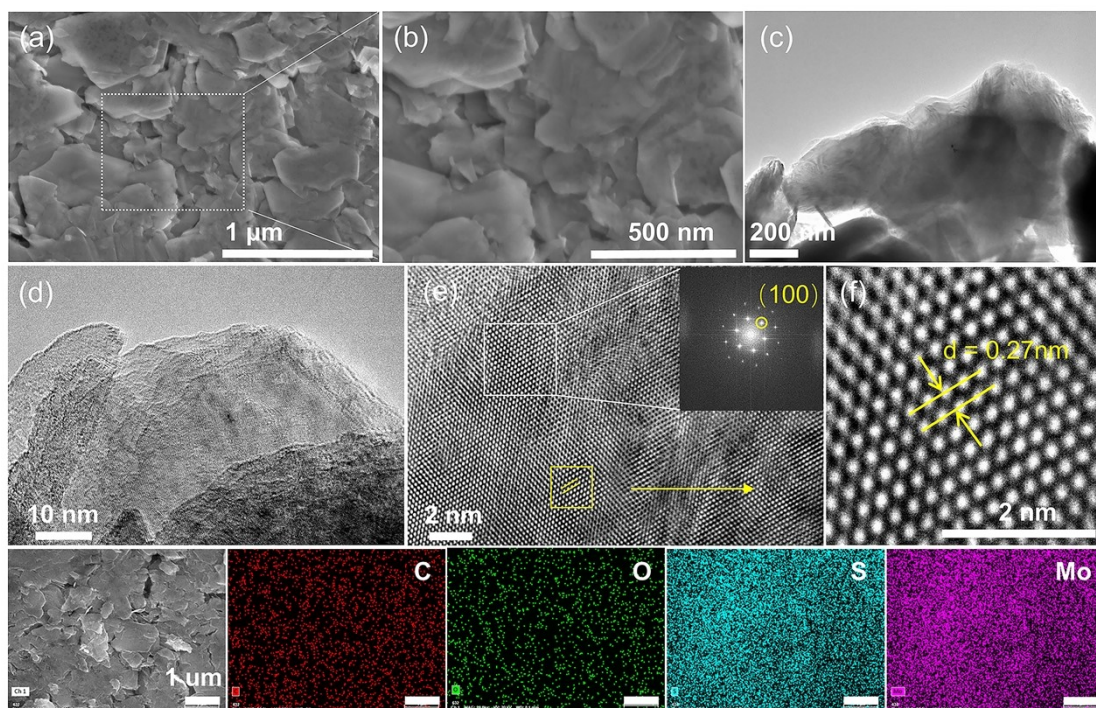


**Fig. S1.** Structural characterization of the pristine MoS<sub>2</sub> sample. (a) and (b) SEM images. (c-e) HRTEM images at different scales and the inset of Fig. (e) is the corresponding FFT pattern. (f) Enlarged image for the selected area. (g). Elemental mapping of C, O, S, and Mo, respectively.

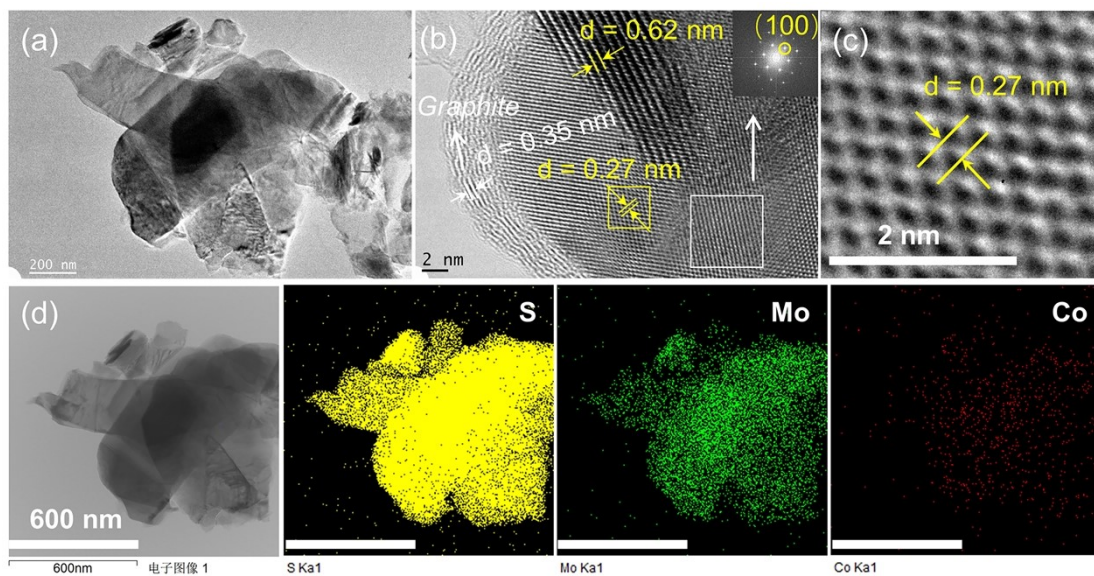


**Fig. S2.** Structural characterization of the Co/MG sample. (a) and (b) HRTEM images at different scales and the inset of Fig. (b) is the corresponding FFT pattern. (c) Enlarged image for the selected area in Fig. (b). (d) Elemental mapping of the S, Mo, and Co, respectively.



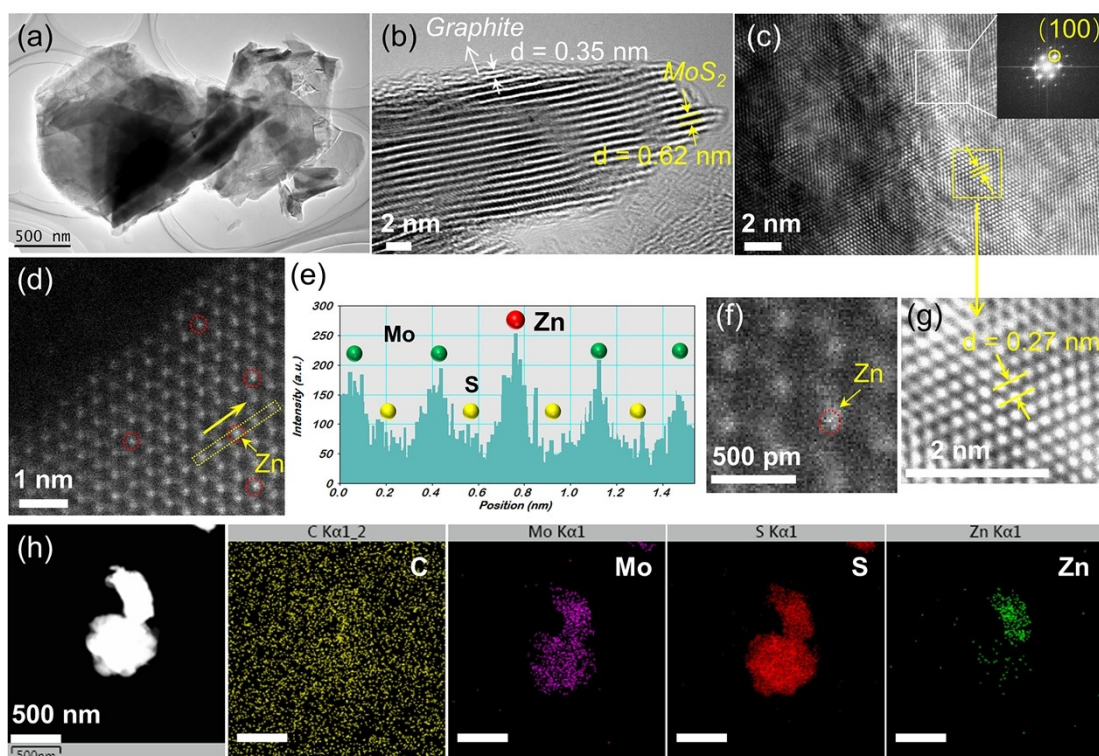


**Fig. S3.** Structural characterization of the Zn/MG sample. (a-c) HRTEM images at different scales and the inset of Fig. (c) is the corresponding FFT pattern. (d) HAADF-STEM image. (e) Intensity profile of the selected line in Fig. (d). (f) Enlarged image of the small area in Fig. (d). (g) HRTEM image of the small area in Fig. (d). (h) Elemental mapping of the C, Mo, S, and Zn, respectively.

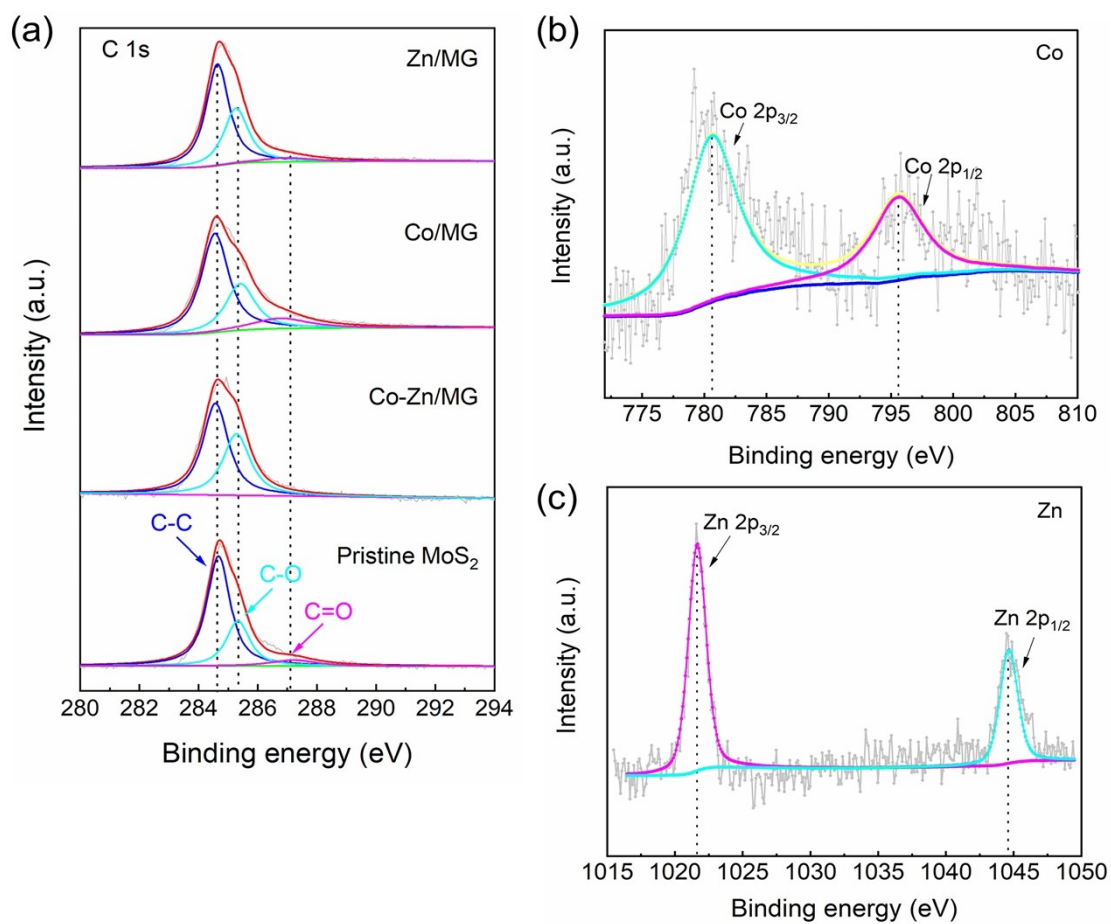


**Fig. S4.** (a) C 1s spectra of the pristine MoS<sub>2</sub>, Co-Zn/MG, Co/MG, and Zn/MG samples. (b) XPS analysis of Co element in the Co/MG sample. (c) XPS analysis of Zn element in the Zn/MG sample.

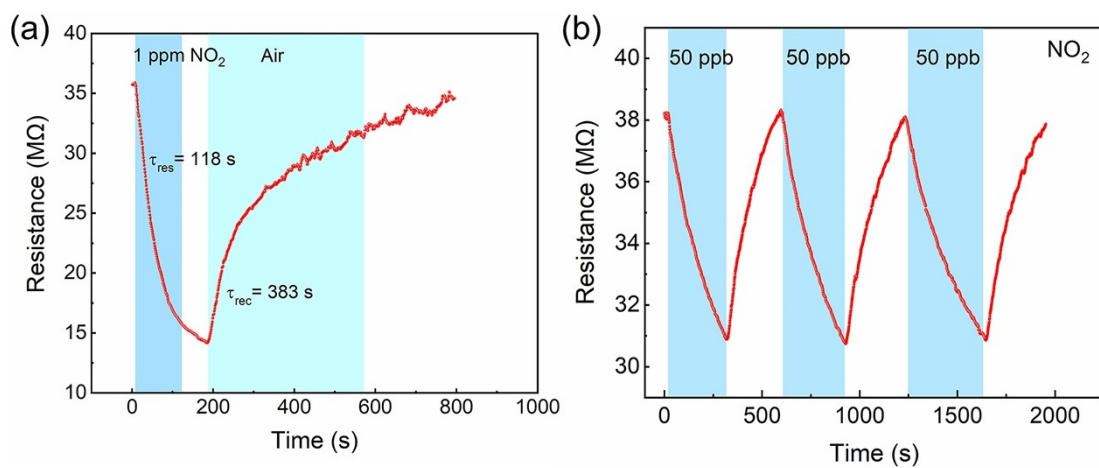


**Fig. S5.** (a) Response-recovery times of the Co-Zn/MG sensor toward 1 ppm NO<sub>2</sub> at RT. (b) Repeatability of the Co-Zn/MG sensor toward 50 ppb NO<sub>2</sub> at RT.

**Table S1.** The calculated reaction rates ( $k$ ) of the sensor for six widely-used gases with a determined concentration at different operating temperatures (Kelvin).

Temp (K)	Type and concentration of gases					
	NO <sub>2</sub> (5 ppm)	NO (5 ppm)	NH <sub>3</sub> (50 ppm)	CO (50 ppm)	H <sub>2</sub> (100 ppm)	Ethanol (50 ppm)
	$k$	$k$	$k$	$k$	$k$	$k$
315.5	0.02522	0.01829	0.00453	0.00941	0.00758	0.00885
323.5	0.02898	0.02	0.00594	0.01273	0.00962	0.01241
342.6	0.03472	0.02534	0.00853	0.01571	0.01278	0.0154
366.7	0.04154	0.03287	0.01381	0.02007	0.01966	0.01998
389.9	0.04975	0.03949	0.01836	0.02514	0.02793	0.03028



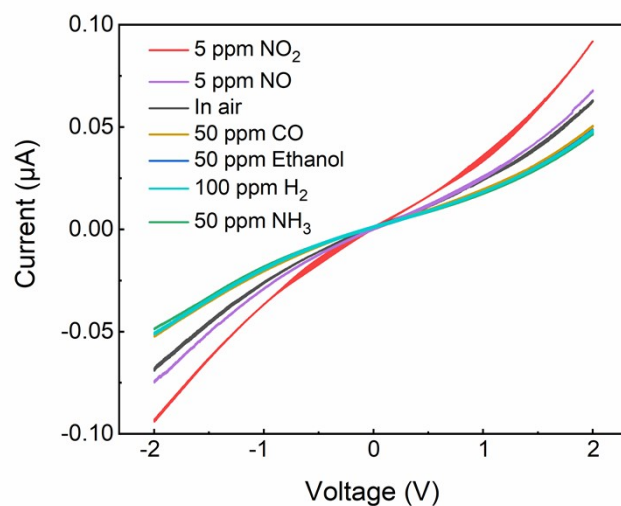


**Fig. S6.** I-V curves of the binary Co-Zn/MG composite sensor under different gas atmospheres measured by the electrochemical workstation (CHI600E, Beijing Join Co. Ltd, China).